Model Selection and Estimation of Multi-compartment Models in Diffusion MRI with a Rician Noise Model

Xinghua Zhu[1], Yaniv Gur[2], Wenping Wang[1], and P. Thomas Fletcher[2]

[1] The University of Hong Kong, Department of Computer Science, Hong Kong
[2] University of Utah, School of Computing, Salt Lake City, UT 84112, USA

Abstract. Multi-compartment models in diffusion MRI (dMRI) are used to describe complex white matter fiber architecture of the brain. In this paper, we propose a novel multi-compartment estimation method based on the ball-and-stick model, which is composed of an isotropic diffusion compartment ("ball") as well as one or more perfectly linear diffusion compartments ("sticks"). To model the noise distribution intrinsic to dMRI measurements, we introduce a Rician likelihood term and estimate the model parameters by means of an Expectation Maximization (EM) algorithm. This paper also addresses the problem of selecting the number of fiber compartments that best fit the data, by introducing a sparsity prior on the volume mixing fractions. This term provides automatic model selection and enables us to discriminate different fiber populations. When applied to simulated data, our method provides accurate estimates of the fiber orientations, diffusivities, and number of compartments, even at low SNR, and outperforms similar methods that rely on a Gaussian noise distribution assumption. We also apply our method to *in vivo* brain data and show that it can successfully capture complex fiber structures that match the known anatomy.

1 Introduction

Diffusion Tensor Imaging (DTI) is a powerful technique that enables inferring white matter pathways of the brain from diffusion weighted (DW) MRI measurements. However, DTI can only describe one dominant diffusion direction per voxel, and therefore, cannot capture known complex fiber structures in the white matter in human brain. The limitation of DTI motivated the development of new imaging modalities that utilize higher angular resolution, as well as new methods to extract white matter structures from such data, including spherical deconvolution [1], Funk-Radon transform [2], multi-compartment models [3, 4], and higher-order tensors [5–7]. In this work, we consider a particular case of multi-compartment models, where the diffusivities in directions perpendicular to the white matter fiber are constrained to be zero. This model is known as the "ball-and-stick", where the "ball" stands for the isotropic diffusion compartment, and each "stick" corresponds to a perfectly linear diffusion compartment (white matter fiber).

J.C. Gee et al. (Eds.): IPMI 2013, LNCS 7917, pp. 644–655, 2013.

The ball-and-stick model was first proposed by Behrens et al. [8] as a constrained version of the multi-tensor model, which comprised only one ball and one stick compartment. A Bayesian framework for the ball-and-one-stick model estimation and tractography was also introduced in [8]. This framework was later elaborated in [9, 4], where multiple anisotropic compartments and model selection methods were proposed. In [9] Hosey et al. focused on the estimation of two-fiber models in a probabilistic manner under Rician noise assumption. They addressed the model selection problem by analyzing the probability density function (PDF) of the Bayes Factor of the one- and two- stick models. On the other hand, the method proposed in [4] did not limit the number of fiber compartments, and the estimation was done under Gaussian noise assumption. They adopted the automatic relevance determination (ARD) algorithm for model selection. However, the model selection methods in [9, 4] did not distinguish two-fiber models from more complicated ones, and no comprehensive evaluation of these methods was reported. More recently, Schultz et al. [11] proposed a spherical deconvolution operation to estimate the fiber orientations and volume fractions, which were refined by fitting a ball-and-stick model to the DW measurements. The number of fibers was selected at the spherical deconvolution level by directly thresholding the associated volume fractions. Similar to [4], this scheme did not account for the Rician noise in the DW measurements. Estimation of the more general two-tensor model, under Rician noise assumption, was presented in [10].

In this paper, the parameters of the ball-and-stick model are estimated by maximizing the log-likelihood function based on the Rician distribution. The maximization problem is solved using an EM algorithm, where the DW measurements with complex Gaussian noise represent the complete data. In addition, in order to find the number of compartments that best fit the data, we use a sparsity prior on the estimated volume fractions. The sparsity prior pushes to zero small volume fractions, and enables elimination of redundant terms that do not represent white matter fibers. In contrast to [9, 10], here we do not restrict our model to two stick compartments, and enable modeling of white matter structures in brain regions that contain up to three fiber populations. The results of the proposed model selection scheme provides a clear distinction between isotropic diffusion, and one, two, or three fiber populations.

The main contributions of this paper can be summarized as follows: 1) We solve the ball-and-stick estimation problem with multiple sticks, under the assumption of Rician noise distribution in the DW measurements. We use a Rician log-likelihood function which is maximized by a robust EM algorithm. 2) We assess the accuracy of our algorithm on simulated data at different b-values and low SNRs, and show that it introduces less bias in the model parameters compared to similar algorithms that rely on a Gaussian noise assumption. 3) We introduce an automatic model selection scheme, which is an integral part of our EM algorithm. This is done by introducing a sparsity prior on the volume fractions. 4) We evaluate the performance of the algorithm on in vivo brain data with deterministic tractography and show its ability to reproduce complex fiber structures matching the known anatomy.

2 Rician Likelihood and Expectation Maximization

In this paper, a parametric partial volume model is used to describe the local diffusion profile. The model we use is known as the "ball-and-sticks", which is composed of a mixture of an isotropic diffusion compartment ("ball"), and multiple directional anisotropic diffusion compartments ("sticks"). The "sticks" correspond to white matter fibers, and are represented by means of the unnormalized *Watson* distribution. That is, given a set of N diffusion weighted measurements, $\{\nu_i\}_{i=1}^N$, for each measurement in a gradient direction $\mathbf{g}_i$, we have

$$\nu_i = S_0 \left\{ w_0 \exp(-b\kappa_0) + \sum_{j=1}^{M} w_j \exp(-b\kappa_j (\mathbf{g}_i^T \mathbf{u_j})^2) \right\}, \tag{1}$$

where M is the number of anisotropic compartments, S_0 is the non-diffusion-weighted signal, and b represents the constant b-value. The model parameters are the white matter fiber orientations, $\mathbf{u}_1, \ldots, \mathbf{u}_M$, diffusion coefficients, $\kappa_0, \ldots, \kappa_M$, and volume fractions, $w_0, \ldots, w_M$, where $\sum_{j=0}^{M} w_j = 1, w_j \geq 0$.

In the rest of this paper, we will denote the set of model parameters by $\Theta = \{\mathbf{u}_1, \ldots, \mathbf{u}_M; w_0, \ldots, w_M; \kappa_0, \ldots, \kappa_M\}$. Also, we will use the notation $\nu_{i0}(\Theta) = S_0 \cdot w_0 \exp(-b\kappa_0)$ to represent the "ball" compartment in the i-th sampled direction, and $\nu_{ij}(\Theta) = S_0 \cdot w_j \exp(-b\kappa_j (\mathbf{g}_i^T \mathbf{u}_j)^2)$ for the j-th "stick" compartment in the i-th sampled direction. Using these notations, the expression for a "clean" signal in measurement direction $\mathbf{g}_i$ is given by the sum of the compartment signals, $\nu_i(\Theta) = \sum_{j=0}^{M} \nu_{ij}(\Theta)$.

2.1 Maximum Rician Likelihood

The MR signal in the complex domain is affected by Gaussian noise. However, the DW measurements are given as the magnitude of the complex MR signal, and, therefore, the noise distribution model becomes Rician. Thus, for a measured DW signal in the i-th gradient direction, S_i, we have $S_i \sim \mathrm{Ric}(\nu_i(\Theta), \sigma)$, given by the PDF

$$p(S_i|\Theta) = \frac{S_i}{\sigma^2} \exp\left(-\frac{S_i^2 + \nu_i(\Theta)^2}{2\sigma^2} \right) I_0\left(\frac{S_i \nu_i(\Theta)}{\sigma^2} \right). \tag{2}$$

We will use the notation $\mathbf{S}$ for the set of observed DW signals, i.e., $\mathbf{S} = \{S_i, i = 1, \ldots, N\}$. Assuming independent measurements in different gradient directions, the joint PDF for the signal $\mathbf{S}$ in each image voxel is given by $p(\mathbf{S}|\Theta) = \prod_{i=1}^{N} p(S_i|\Theta)$. We estimate the parameters Θ by maximization of the likelihood $l(\Theta|\mathbf{S}) = \log p(\mathbf{S}|\Theta)$, which is given by

$$l(\Theta|\mathbf{S}) = -2N \log(\sigma) + \sum_{i=1}^{N} \log(S_i) - \frac{S_i^2 + \nu_i(\Theta)^2}{2\sigma^2} + \log I_0\left(\frac{S_i \nu_i(\Theta)}{\sigma^2} \right). \tag{3}$$

2.2 Expectation Maximization Algorithm

One may apply a gradient ascent method to maximize the log-likelihood function. However, when directly maximizing $l(\Theta|\mathbf{S})$, the optimization parameters are variables of the modified Bessel function I_0. On the other hand, the proposed EM algorithm does not involve the computation of I_0 and its derivatives with respect to the optimization parameters. Therefore, maximizing the Q-function in the E-step is more stable numerically, and more tractable in terms of the analytical computations involved. Indeed, we have found that the proposed EM algorithm provides more accurate estimates of the model parameters.

Let us now consider a mixture model of one "ball" compartment and M different "stick" compartments. In the complex domain, the signal generated by the jth compartment in the ith sampled direction is corrupted by complex Gaussian noise, such that

$$Y_{ij} = \nu_{ij}(\Theta) + \epsilon, \quad \epsilon \sim \mathcal{CN}\left(0, \frac{2\sigma^2}{M+1}\right), \tag{4}$$

where $\mathcal{CN}$ denotes the circularly-symmetric complex normal distribution. Therefore, the PDF and log-likelihood of the complex signal, Y_{ij}, given Θ are

$$p(Y_{ij}|\Theta) = \frac{1}{2\pi\sigma^2/(M+1)} \exp\left(-\frac{\|Y_{ij} - \nu_{ij}(\Theta)\|^2}{2\sigma^2/(M+1)}\right), \tag{5}$$

$$l(\Theta|\{Y_{ij}\}) = \sum_{i=1}^{N}\sum_{j=0}^{M} -\log(2\pi\sigma^2/(M+1)) - \frac{\|Y_{ij} - \nu_{ij}(\Theta)\|^2}{2\sigma^2/(M+1)}. \tag{6}$$

Note that the complex signal, Y_{ij}, represent the complete data in our EM algorithm, whereas the observed incomplete data is the magnitude of a mixture of complex signals, that is $S_i = \left\|\sum_{j=0}^{M} Y_{ij}\right\|$, where $S_i \sim \text{Ric}\left(\nu_i(\Theta), \sigma^2\right)$ [12].

The E-step is derived by calculating the expected value of the log-likelihood with respect to the complete data $\mathbf{Y} = \{Y_{ij}, i = 1, \ldots, N, j = 0, \ldots, M\}$:

$$Q(\Theta|\Theta^{(k)}) = E\left[l(\Theta|\mathbf{Y})|\mathbf{S}, \Theta^{(k)}\right] = \int l(\Theta|\mathbf{Y}) p(\mathbf{Y}|\mathbf{S}, \Theta^{(k)}) d\mathbf{Y}. \tag{7}$$

Following some extensive derivations, which are too lengthy to be included in this paper, we arrive at the final expression for the Q-function:

$$Q(\Theta|\Theta^{(k)}) = \sum_{i,j} 2\nu_{ij}(\Theta)\left[\frac{S_i}{M+1} A\left(\frac{S_i\nu_i^{(k)}}{\sigma^2}\right) - \frac{\nu_i^{(k)}}{M+1} + \nu_{ij}^{(k)}\right] - \nu_{ij}(\Theta)^2,$$

where $A(x) = I_1(x)/I_0(x)$, $\nu_i^{(k)} = \nu_i(\Theta^{(k)})$, $\nu_{ij}^{(k)} = \nu_{ij}(\Theta^{(k)})$.

In the M-step, the model parameters Θ are updated to maximize Q via gradient ascent. The partial derivative of Q with respect to $\theta \in \Theta$ is given by

$$\frac{dQ}{d\theta} = 2\sum_{i,j}\left[\frac{S_i}{M+1} A\left(\frac{S_i\nu_i^{(k)}}{\sigma^2}\right) - \frac{\nu_i^{(k)}}{M+1} + \nu_{ij}^{(k)} - \nu_{ij}(\Theta)\right]\frac{d\nu_{ij}}{d\theta}. \tag{8}$$

The derivatives $d\nu_{ij}/d\mathbf{u}_j$ are computed in the tangent space of the real projective space, $\mathbb{RP}^2$, i.e., the space of bi-directional unit vectors, due to the antipodal symmetry of diffusion. We write the stick components ν_{ij} in terms of the geodesic distance on $\mathbb{RP}^2$, that is, $\cos d(\mathbf{g}_i, \mathbf{u}_j) = \mathbf{g}_i^T \mathbf{u}_j$. This leads to

$$\frac{d\nu_{ij}(\Theta)}{d\mathbf{u}_j} = -w_j S_0 \exp(-b\kappa_j(\cos d(\mathbf{g}_i, \mathbf{u}_j))^2) \frac{b\kappa_j \sin 2d(\mathbf{g}_i, \mathbf{u}_j)}{d(\mathbf{g}_i, \mathbf{u}_j)} \mathrm{Log}_{\mathbf{u}_j}(\mathbf{g}_i)$$

The derivatives $d\nu_{ij}/dw_j$ and $d\nu_{ij}/d\kappa_j$ are straightforward to compute and are not included here. These derivatives, combined with the expression in (8), define the update step in the gradient ascent in the M-step.

3 Sparsity Prior on Compartment Fractions

When fitting to a noisy DW signal with unknown number of fiber compartments, an increase in the number of sticks will generally improve the model fit. However, increasing the number of sticks beyond the true number of fiber compartments will overfit to the imaging noise. In real applications, we favor representation of a diffusion profile with as few compartments as possible. In terms of the parameters, this means we favor weighting fractions that concentrate on a minimal number of necessary compartments, rather than distribute equally upon all compartments. Therefore, we introduce a sparsity prior for the compartment fractions.

The l_p-norm with $p \leq 1$ is universally used as a sparsity (or concentration) measure, where the most common choice being the l_1-norm. However, the l_1-norm of the volume fractions $\|(w_0, \ldots, w_M)\|_1 = \sum_{j=0}^{M} w_j$ is constrained to be 1 in our case and cannot reflect sparsity level. Alternatively, we use the $l_{0.5}$-norm as the sparsity measure. That is,

$$\mathcal{C}(w_0, w_1, \ldots, w_M) = \left(\sum_{j=0}^{M} w_j^{0.5} \right)^2, \tag{9}$$

where $\mathcal{C}$ gets its maximal value when all the fractions are equal, and its minimal value when one fraction equals to 1 and the rest equal to zero.

This term penalizes the number of compartments such that when a volume fraction, w_j, tends to zero during the optimization process, the derivative $d\mathcal{C}/dw_j$ tends to negative infinity, which results in pushing w_j faster toward zero. In that case, the value of w_j cannot increase anymore, the associated stick compartment will no longer correspond to a white matter fiber, and will be eliminated from the optimization process. We treat the sparsity penalty defined by (9) as a negative log prior on volume fractions, which results in an amended Q function

$$\hat{Q}(\Theta|\Theta^{(k)}) = Q(\Theta|\Theta^{(k)}) - \lambda_C \cdot \mathcal{C}(w_0, \ldots, w_M), \tag{10}$$

where λ_C is a tunable coupling factor for the sparsity constraint. Thus, in the maximization step in the EM algorithm, the derivative of $\mathcal{C}$ is included in the gradient ascent update of the volume fractions.

4 Implementation Details

4.1 Initialization and Model Selection

In the proposed algorithm, the number of stick compartments is automatically selected using the sparsity constraint.

At the beginning of the estimation, the number of stick compartments is set to 3. A 2nd-order tensor is fit to the DW signal and its eigenvectors and eigenvalues are used to initialize the stick directions and diffusivity, respectively. Initial volume fractions are set to 0.25 equally for all stick and ball compartments.

During estimation, compartments with fractions driven to zero by the sparsity constraint are instantly removed from the model. In cases where small fractions of redundant compartments remain in the estimation results when the EM algorithm converges, a set of predefined fraction thresholds, W_1, W_2, and W_3, are applied to remove them. Given K stick compartments, those with fractions $w_j < W_K$ would be removed from the estimated model. If one or more compartments are removed by thresholding, the EM is continued with the reduced model until convergence again. Otherwise, the compartment number is determined. We then set $\lambda_C = 0$ and let the EM converge again, in order to eliminate the bias introduced by the sparsity constraint.

In our experiments, a universal set of fraction thresholds, $W_1 = 0.15$, $W_2 = 0.1$, and $W_3 = 0.05$, are used in all scenarios. These values are empirically selected from repetitive experiments and found to provide plausible results in synthetic data with various settings. The coupling factor, λ_C, can be set with respect to different b-value and SNR scenarios. In particular, we tune the value of λ_C to perform optimally on simulated training data (independent from the testing data in the results section) with the given b-value and SNR.

4.2 Assumptions on Diffusivity

It is known that indeterminacy prevents simultaneous estimation of diffusivities and volume fractions when the DW measurements are available for a single b-value only [13]. As we use the volume fractions for automatic model selection, constraining assumptions are made on diffusivity values to resolve parameter indeterminacy.

We first assume that the ball diffusivity is known and constant in a dataset, and let the algorithm determine the optimal fraction of the ball compartment for a given diffusivity. In practice, even though the ball diffusivity and volume fraction are in-determinant for a single voxel, we can estimate a common ball diffusivity from a *collection* of voxels. We discuss this process in the next section.

Secondly, we assume that all stick compartments in one voxel have the same diffusivity. This assumption helps to distinguish stick compartments from the ball. A stick compartment degenerates into a ball compartment when its diffusivity approaches zero. With this constraint, when a stick compartment is redundant, the EM algorithm inclines to decrease its fraction instead of its diffusivity, so it prevents the emergence of an additional isotropic compartment.

4.3 Estimating Ball Diffusivity

As the ball diffusivity is assumed to be known in the proposed estimation algorithm, its value needs to be determined from the given data. Yet, when the ball diffusivity and fraction are both unknown, indeterminacy between the two parameters prevents reliable estimation of either of them. To solve this problem, based on the assumption that the true ball diffusivity is constant in the dataset, we propose the following procedure to estimate its value. We first select a number of voxels with a single-fiber configuration. Then, we fit a ball-and-one-stick model to these voxels by alternating between estimating the diffusivities and the volume fractions, with the other fixed. After each iteration, the median of the diffusivities / fractions among all selected voxels are used to initiate the next round of estimation. After a few iterations, the median values would converge and the median ball diffusivity at convergence is taken as the ball diffusivity for the given dataset.

5 Results

5.1 Simulated Data

First, we tested the performance of the proposed method on simulated data. The clean DW measurements were synthesized using the ball-and-stick model with 64 gradient directions. In the simulation, all ball and stick compartments had the same volume fraction, $1/(M+1)$, where M was the number of stick compartments simulated. The stick and ball diffusivities were derived to closely simulate real white matter and were set as 1.54×10^{-3} and 8.83×10^{-4}, respectively. The simulated DW signal was corrupted by Rician noise using a standard procedure where a complex Gaussian noise was added to the signal, and we took the modulus of the noisy signal in the complex domain.

The proposed method was evaluated at b-values of 2000 and 3000, and baseline SNRs of 15 and 20. For each scenario 100 noisy signal instances were generated to gather statistical evaluation of the estimation performance.

For each pair of b-value and SNR, we randomly picked 50 samples from the single-fiber signals and applied the method described in Section 4.3 to recover the ball diffusivity.

Parameter Estimation Accuracy. We assessed the accuracy of our algorithm in various cases that differed by the separation angle and the number of simulated compartments. We compared our results with the ball-and-stick estimation scheme proposed by Schultz et al. [11]. Also, to compare the reconstruction behavior between Rician and Gaussian noise models, we implemented a variant of our method where the Rician likelihood was replaced with the *Gaussian* likelihood. In this experiment, we fixed the number of stick compartments in both the algorithm of [11] and our algorithm (and, thus, turned off the sparsity prior by setting $\lambda_C = 0$).

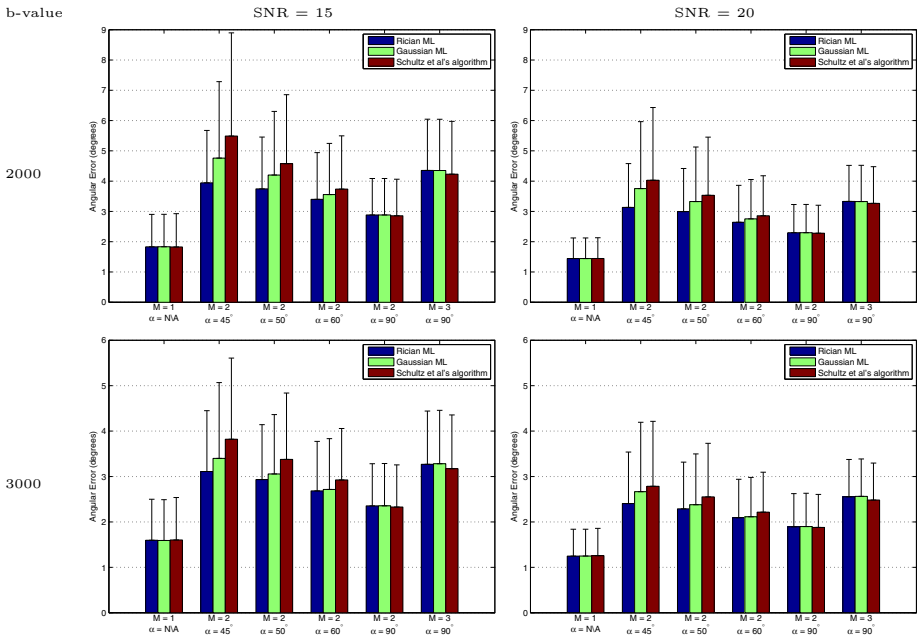

Fig. 1. Angular error of estimated stick directions (mean and standard deviation)

Figs. 1 and 2 show the errors in estimated stick directions and diffusivities, where M and α stand for the number of simulated compartments and the (minimum) separation angle between stick directions, respectively. When the separation angle is low, our method shows less bias in fiber orientations compared to the other two approaches. As the separation angle increases, or when there is only one stick component, the three methods perform similarly. As for diffusivity estimation, the proposed Rician ML algorithm consistently outperforms its opponents. Schultz et al.'s algorithm uses the same diffusivity for both ball and stick compartments, which would not adapt to the simulated situation, and therefore presents large diffusivity errors. Although the Gaussian and Rician ML methods perform similarly in terms of angular deviation in high-separation-angle scenarios, the Gaussian ML is less accurate in diffusivity estimation, due to the bias inherent to using a Gaussian approximation to the Rice distribution.

Model Selection. Now, we assume that the number of compartments is not known, and determine its value using the sparsity constraint on the volume fractions, as described in Section 4.1. The performance of the sparsity constraint was tested with both Rician and Gaussian noise models. The coupling factor, λ_C, ranged between 20 to 40, was chosen according to the b-value and SNR, using independent synthetic training data. The success rate of compartment number estimation is shown in Table 1. In most cases, the Rician model outperforms the

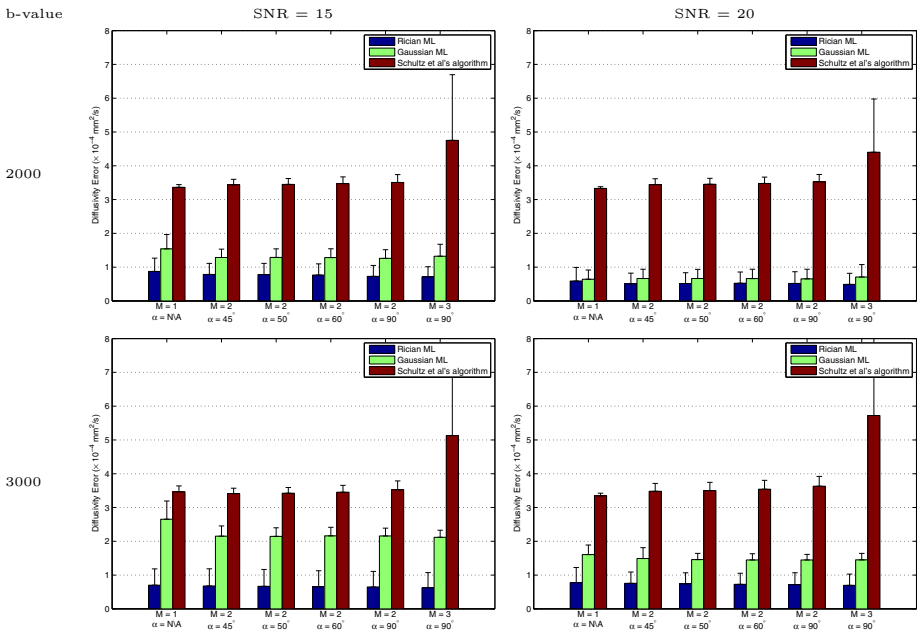

Fig. 2. Root mean square error of the estimated diffusivities

Gaussian one, especially at low SNRs. The only cases where the Gaussian ML performs better are at SNR=20 and a separation angle of 45°.

In addition, we compared the proposed model selection method with the Akaike Information Criteria (AIC). As shown in Table 1, AIC produces plausible results only for isotropic, or single fiber configurations. It is found that AIC is very conservative in choosing the optimal number of parameters, such that it always underestimates the number of compartments for complex diffusion structures. We have also found that the similar Bayesian Information Criteria (BIC) is even more conservative than the AIC.

5.2 In Vivo Brain Data

The human brain data was acquired on a 3T Siemens Allegra Tim Trio scanner using a b-value of 2000 s/mm^2. The scan was composed of 10 B0 volumes and 60 diffusion weighted volumes of matrix size $128 \times 128 \times 70$, and voxel size of $2 \times 2 \times 2$ mm^3. The volumes were registered to a T_1 template with a voxel size of 1 mm^3, and corrected for motion, eddy current, and EPI distortions. The Rician noise parameter σ was estimated from background voxels as $\hat{\sigma} = \sqrt{\text{var}(S)/2}$. To determine the ball diffusivity in the brain data, 50 voxels were selected in the corpus callosum region, where the number of sticks was known to be 1. Following the procedure in Section 4.3, the ball diffusivity was estimated as 8.8294×10^{-4}.

We selected a $41 \times 41 \times 41$ region of the brain data for experimental evaluation. In the selected region, the SNR was estimated to be approximately 25. We chose

Table 1. Accuracy of number of compartments determination (in percentage)

	Compartment no.		0	1	2				3
	Separation angle		-	-	45°	50°	60°	90°	90°
Rician ML w/ Sparsity Prior	b-value = 2000	SNR=15	98	**100**	**75**	**95**	**100**	**100**	**100**
		SNR=20	**100**	**100**	83	**99**	**100**	**100**	**100**
	b-value = 3000	SNR=15	**100**	**100**	**72**	**96**	**98**	**100**	**100**
		SNR=20	**100**	**100**	71	**98**	**100**	**100**	**100**
Gaussian ML w/ Sparsity Prior	b-value = 2000	SNR=15	**100**	84	73	74	73	69	**100**
		SNR=20	**100**	96	**90**	91	90	86	**100**
	b-value = 3000	SNR=15	**100**	85	71	77	77	74	**100**
		SNR=20	**100**	96	**89**	91	93	93	**100**
Rician ML w/ AIC	b-value = 2000	SNR=15	**100**	**100**	0	0	0	29	0
		SNR=20	**100**	**100**	0	0	0	99	0
	b-value = 3000	SNR=15	**100**	**100**	0	0	0	83	0
		SNR=20	**100**	**100**	0	0	8	**100**	15

the sparsity prior coupling factor $\lambda_C = 75$ using a few synthesized training samples of the same b-value and SNR.

Figure 3(a) and (b) show the parameter estimation and automatic model selection results with the proposed method. It is easy to identify the corpus callosum where the one-stick model was selected, with a clear boundary against the isotropic background. Meanwhile, the 3-stick model was selected in the crossing region of the corpus callosum, cortical spinal and SLF. The pattern of the number of sticks is highly consistent with known anatomy of the white matter in the brain. Some erroneous model selection results can be spotted in the CSF, and at the boundary between the CSF and the white matter tracts, where 3 sticks are attributed. This is likely to result from an underestimated ball diffusivity.

As a comparison, we used the voxel classification method in Camino [14] to select the optimal order of spherical harmonics for the diffusion data, which applied Alexander et al.'s algorithm using an F-test [15]. In this method, three classes are detected with corresponding spherical harmonics orders 0, 2, and 4, which stand for isotropic diffusion, single directional diffusion tensor, and complex diffusion structures consisting of two or more fiber orientations, respectively. We set the background signal threshold as 100 and the thresholds for separating the three classes as 1×10^{-20}, 1×10^{-6} and 1×10^{-6}. As shown in Figure 3(d), the output of the F-test is noisy and does not match the anatomy well, especially in the crossing region of the three tracts.

We used the deterministic tractography tool in Camino to perform fiber tracking from our reconstruction results. The fibers were seeded in every voxel where our method detected one or more stick compartments. Following the tractography process, ROIs were used separately to select fiber bundles in the corpus callosum, cortical spinal and SLF, respectively, as shown in Figure 3(e) - (g). For the corpus callosum, tractography from the reconstructed ball-and-stick model reproduced the U-shaped callosal radiation and also the lateral transcallosal

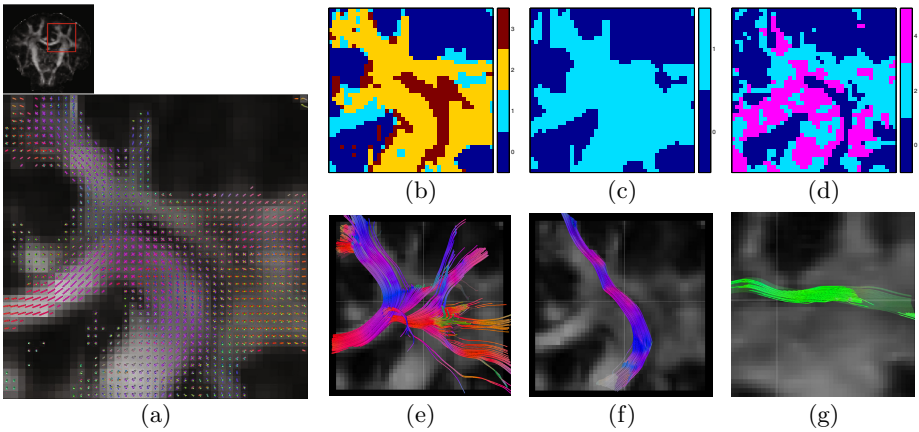

Fig. 3. Automatic model selection and reconstruction results on in vivo brain data. (a) Location of the selected section and the stick orientations (weighted by associated fractions) reconstructed with the proposed method; (b) stick compartment numbers estimated with the proposed method; (c) stick compartment numbers estimated with AIC; (d) the order of spherical harmonics selected by F-test; (e) - (g) tractography results from the reconstructed ball-and-stick models for (e) corpus callosum, (f) cortical spinal, and (g) SLF (sagittal slice).

fibers. In addition, the tractography yielded the cortical spinal going from bottom to top, as well as the SLF bundle in the front-back direction. All the three tracts crossed at the center region of the depicted section.

6 Conclusions

In this paper, we proposed a novel scheme for estimating parameters in a multi-compartment model that is composed of an isotropic "ball" compartment, and multiple perfectly linear "stick" compartments, under Rician noise assumption. Our scheme combines a robust Rician EM algorithm, and a sparsity prior on the volume mixing fractions to automatically select the number of compartments. Using simulated data, we showed that our formulation reduces bias in the estimation of fiber orientations, diffusivities, and number of compartments, compared to alternative schemes that rely on a Gaussian noise assumption. Furthermore, we applied the proposed algorithm to in vivo brain data and show that our method provides a clear distinction between different fiber populations, and is able to reconstruct fiber pathways that match known white matter structures such as the transcallosal fibers.

Acknowledgements. This project was supported in part by grants R01 MH084795, 5P41RR012553-14, and 8P41GM103545-14 from the National Institutes of Health.

References

1. Tournier, Calamante, F., Gadian, D.G., Connelly, A.: Direct estimation of the fiber orientation density function from diffusion-weighted MRI data using spherical deconvolution. NeuroImage 23(3), 1176–1185 (2004)
2. Descoteaux, M., Angelino, E., Fitzgibbons, S., Deriche, R.: Regularized, fast, and robust analytical Q-ball imaging. Magn. Res. Med. 58(3), 497–510 (2007)
3. Tuch, D.S., Reese, T.G., Wiegell, M.R., Wedeen, V.J.: Diffusion MRI of Complex Neural Architecture. Neuron 40(5), 885–895 (2003)
4. Behrens, T.E., Berg, H.J., Jbabdi, S., Rushworth, M.F., Woolrich, M.W.: Probabilistic diffusion tractography with multiple fibre orientations: What can we gain? NeuroImage 34(1), 144–155 (2007)
5. Liu, C., Bammer, R., Acar, B., Moseley, M.E.: Characterizing non-gaussian diffusion by using generalized diffusion tensors. Magn. Reson. Med. 51(5), 924–937 (2004)
6. Weldeselassie, Y.T., Barmpoutis, A., Atkins, M.S.: Symmetric positive-definite cartesian tensor orientation distribution functions (CT-ODF). In: Jiang, T., Navab, N., Pluim, J.P.W., Viergever, M.A. (eds.) MICCAI 2010, Part I. LNCS, vol. 6361, pp. 582–589. Springer, Heidelberg (2010)
7. Jiao, F., Gur, Y., Johnson, C.R., Joshi, S.: Detection of crossing white matter fibers with high-order tensors and rank-k decompositions. In: Székely, G., Hahn, H.K. (eds.) IPMI 2011. LNCS, vol. 6801, pp. 538–549. Springer, Heidelberg (2011)
8. Behrens, T.E.J., Woolrich, M.W., Jenkinson, M., Johansen-Berg, H., Nunes, R.G., Clare, S., Matthews, P.M., Brady, J.M., Smith, S.M.: Characterization and propagation of uncertainty in diffusion-weighted MR imaging. Magn. Reson. Med. 50(5), 1077–1088 (2003)
9. Hosey, T., Williams, G., Ansorge, R.: Inference of multiple fiber orientations in high angular resolution diffusion imaging. Magn. Reson. Med. 54(6), 1480–1489 (2005)
10. Caan, M., Khedoe, H., Poot, D., den Dekker, A., Olabarriaga, S., Grimbergen, K., van Vliet, L., Vos, F.: Estimation of diffusion properties in crossing fiber bundles. IEEE Transactions on Medical Imaging 29(8), 1504–1515 (2010)
11. Schultz, T., Westin, C.-F., Kindlmann, G.: Multi-diffusion-tensor fitting via spherical deconvolution: A unifying framework. In: Jiang, T., Navab, N., Pluim, J.P.W., Viergever, M.A. (eds.) MICCAI 2010, Part I. LNCS, vol. 6361, pp. 674–681. Springer, Heidelberg (2010)
12. Marzetta, T.L.: EM algorithm for estimating the parameters of a multivariate complex Rician density for polarimetric SAR. In: 1995 International Conference on Acoustics, Speech, and Signal Processing, vol. 5, pp. 3651–3654. IEEE (1995)
13. Scherrer, B., Warfield, S.K.: Why multiple b-values are required for multi-tensor models. Evaluation with a constrained log-Euclidean model. In: Proc. of the 7th IEEE International Symposium on Biomedical Imaging (ISBI), pp. 1389–1392 (2010)
14. Cook, P., Bai, Y., Nedjati-Gilani, S., Seunarine, K., Hall, M., Parker, G., Alexander, D.: Camino: Open-source diffusion-mri reconstruction and processing. In: 14th Scientific Meeting of the International Society for Magnetic Resonance in Medicine, vol. 2759 (2006)
15. Alexander, D., Barker, G., Arridge, S.: Detection and modeling of non-gaussian apparent diffusion coefficient profiles in human brain data. Magnetic Resonance in Medicine 48(2), 331–340 (2002)